The variation of surface propensity of halides with droplet size and temperature; The planar interface limit

Victor Kwan,[†] Styliani Consta,[*,†] and Shahrazad M. A. Malek[‡]

† *Department of Chemistry, The University of Western Ontario, London, Ontario, Canada N6A 5B7*

‡ *Department of Physics and Physical Oceanography, Memorial University of Newfoundland, Canada, A1B 3X7*

E-mail: sconstas@uwo.ca

Abstract

The radial number density profiles of halide and alkali ions in aqueous clusters with equimolar radius $\lessapprox$ 1.4 nm, that correspond to $\lessapprox$255 H_2O molecules, have been extensively studied by computations. However, the surface abundance of Cl^-, Br^- and I^- relative to the bulk interior in these smaller clusters may not be representative of the larger systems. Indeed, here we show that the larger the cluster is, the lower the relative surface abundance of chaotropic halides is. In droplets with equimolar radius of $\approx$ 2.45 nm that corresponds to $\approx$ 2000 H2O molecules, the polarizable halides show a number density maximum in the droplet's bulk-like interior. A similar pattern is observed in simulations of the aqueous planar interface with halide salts at room temperature. At elevated temperature the surface propensity of Cl^- decreases gradually, while that of I^- is partially preserved. The change of the chaotropic halide location at higher temperatures relative to room temperature may considerably affect photochemical reactivity in atmospheric aerosols, vapor-liquid nucleation and growth mechanisms, and salt crystallization via solvent evaporation. We argue that the commonly used approach of nullifying parameters in a force field in order to find the factors that determine the ion location does not provide transferable insight to other force fields.

Introduction

Aqueous droplets containing alkali and halide ions are omni-present in atmospheric aerosols[1–8] and man-made sprays often used in technology and as ionization methods in analytical chemistry. It is important to know the ions' relative abundance in the interface because as expected, water molecules and ions in this region are more readily available for chemical reactions including catalysis[9,10] with incoming species and evaporation than the bulk interior.[3,11,12] In addition, ions can serve as nucleation centers in the vapor or in the liquid-ice phase transition, and in this role their surface affinity may affect the nucleation mechanisms and rates.[13,14] Hereafter, we will use the term "cluster" and "droplet" interchangeably.

The variation in a droplet's size that may lead to systems with different physical and chemical properties has been a focus of many studies. Studies of vapor-water planar interfaces[4,7,15–29] may provide insight into the chemistry in the interface of neutral macroscopic clusters (droplets) or solid particles.[12,30–56] Nevertheless, an ion without neutralizing counterions in a droplet is subject to different forces from those in a planar interface because the

spherical geometry enters the boundary conditions in the electostatic equations as we discuss in the next paragraphs.

There is also a significant amount of theoretical and experimental research that investigates the local minima in the potential energy surface and free energy of solvation of a single alkali or halogen ion embedded in clusters.[57–82] The topic is still investigated in order to reconcile differences between computations and experiments and achieve detailed modeling mainly in the smallest clusters via the use of high level quantum chemistry calculations.[83–87]

The location of halide and alkali ions in aqueous clusters, has been considered a resolved matter in the literature. Studies over several decades have reached consensus that the number density of a single Cl^-, Br^-, I^- is enhanced in the surface region, and that of F^- and alkali ions shows a broad maximum in the droplet's center of mass.[4,21,58,62,63,67,88–93] However, the number density profiles of the halide ions as a function of droplet size and their proximity to the ion distributions in the planar interface is still unexplored. Moreover, studies of the number density and solvation of ions in nanodroplets at cold temperatures or elevated temperatures relative to room temperature are still limited.[73,74,91] The studies at elevated temperature are more relevant nowadays for atmospheric processes since the temperature in Earth shifts toward higher values.

All the computational studies so far have been performed for clusters composed of a few tens of H_2O molecules, or for clusters with approximately 190 - 255 H_2O molecules using polarizable and non-polarizable models. Perera et al.[91] studied clusters with 238 H_2O molecules, Stuart and Berne,[89] up to 255 H_2O molecules using OPLS (optimized potential for liquid state) and a charge fluctuating model, Caleman et al.[92] $\approx$ 200 H_2O molecules using a Drude oscillator-based polarizable model.[94] Stuart and Berne attempted to find the cluster size at which a sole Cl^- ion would transfer in the interior by extrapolating from clusters of up to $\leq$ 255 H_2O molecules.[89] However, the extrapolation could not make a clear prediction and the question remained open. To explain the ion surface propensity, factors that have been examined are the ion and water polarization, charge and ion size.[56,88] Stuart and Berne established that Cl^- is located near the surface when a polarizable water model is used and in the cluster interior when a non-polarizable model is used.[89] Wick and Xantheas reported simulations of ions in a slab geometry using a polarizable force field.[90] They considered the factors of size and polarizability for I^- and Cl^-. They found anisotropy in the solvation structure of the ions, which correlated with polarizability.

Our reference point for the location of a point charge in a droplet is that the number density peaks at the droplet's center of mass (COM). This number density profile is predicted by an analytical model that we developed,[74,95] which finds that a point charge in a spherical droplet (where shape fluctuations have been considered) is always subject to a harmonic potential centered at the droplets' COM. We named this effect electrostatic confinement (EC).

In EC, the energy, ΔE_1, related to the distance of the ion from the droplet's COM is given by

$$\Delta E_1(\|\mathbf{r}\|) = K(\varepsilon)\frac{Q^2}{R^3}\|\mathbf{r}\|^2 \tag{1}$$

where

$$K(\varepsilon) = \frac{\varepsilon - 1}{4\pi\epsilon_0\varepsilon(\varepsilon + 2)} \tag{2}$$

Q, R and ε are the charge of the ion, the droplet radius and the relative dielectric constant of the solvent, respectively, ϵ_0 is the vacuum permittivity and $\|\mathbf{r}\|^2 = X_{\mathrm{COM}}^2 + Y_{\mathrm{COM}}^2 + Z_{\mathrm{COM}}^2$ (where $X_{\mathrm{COM}}, Y_{\mathrm{COM}}, Z_{\mathrm{COM}}$ are the coordinates of the droplet's COM). The center of the droplet is placed on the ion.

The EC is more evident for an ion with a charge of at least $\pm 3e$ (where e is the elementary positive charge) found in a droplet with a relatively small radius. For the EC to become evident the radius size will be equal or moderately larger than the radius at the Rayleigh limit.[96–98] The Rayleigh limit is defined as the point where the electrostatic forces balance the surface forces in a droplet. In small droplets the geometric confinement may compete with EC, and then the single ion number density becomes uniform within the droplet's interior.

Even though, EC is always present, chemical factors such as charge transfer may mask its effect. A simple view of the location of F^- and alkali ions shows consistency with EC possibly due to their small size. The polarizable halides are more complicated because of their large size and polarization. Onsager-Samaras (OS) theory[45,99–101] is often used for explaining the repulsion of the ions from the interface. The fundamental electrostatic treatment of the problem is almost the same in the EC and OS theory, with the difference that in OS the linearized Poisson-Boltzmann equation is used vs. the non-linearized equations used in EC. Studies in aqueous planar interfaces have demonstrated the deviation from OS, and thus, the need for atomistic modeling or additional terms in the analytical theory. A molecular-level approach considers the following free energy contributions that may determine the ion location:[45,100,102] (a) The hydrophobic effect that arises from the ion size. This effect leads to a free energy penalty to create a cavity within the H_2O network. This factor favors the ion solvation in the subsurface and surface. (b) The ion solvation due to charge and its sign. An ion in the interface may be partially solvated, which leads to a free energy penalty relative to the completely solvated state. This factor favors the ion location in the subsurface and interior. (c) The interaction of the ion with the surface potential[28,103–106] of H_2O. The polarity of the H_2O molecules in the interface in combination with the orientation of the H_2O molecules surrounding the ion may lead to the ion attraction or repulsion in the vapor-liquid interface. The explicit electronic polarization of the ions and H_2O may reinforce factors (b) and (c). In this manuscript we hypothesize that as the droplet size or temperature increases the halide number density shifts toward the droplet interior because of reduced interaction between the polarizable ion and the surface potential.

Systems and simulation methods

Molecular dynamics (MD) simulations of charged aqueous droplets containing a sole anion F^-, Cl^-, Br^- and I^- were performed. For comparison, simulations have also been performed with Cs^+.

The majority of the simulations in this study have been performed with the polarizable model[94] SWM4-NDP with the CHARMM-Drude force field.[110] The ion parameters are shown in Table S1 in SI. Hereafter, the model will be denoted as "Drude". The systems and characteristics of their structure using the Drude model are described in Table 1.

For comparison, three non-polarizable parameter sets were also used. The non-polarizable models are: (a) the TIP4P/2005 water model[111] with the ion parameters from OPLS-AA,[112,113] denoted hereafter as OPLS; (b) exactly the same model as in (a), but the charge of the ions are scaled by a factor of 0.75 suggested by Kirby and Jungwirth,[114] denoted hereafter as OPLS‡; and (c) TIP4P/2005[111] water model with the Madrid-2019-Extended ion parameters,[115,116] where the ions are scaled by a factor of 0.85, denoted hereafter as M19. The charge-scaling models intend to provide a mean field treatment of polarizability.

The majority of the simulations have been performed for aqueous droplets ranging in size between $N = 200$ ($R_e = 1.1$ nm, where R_e denotes the equimolar radius) to $N = 2000$ ($R_e = 2.45$ nm). Only for Cl^- and I^- simulations using the Drude model were performed in a 6000 H_2O droplet ($R_e = 3.55$ nm).

The MD simulations were performed in the canonical ensemble using NAMD version 2.14.[117] The droplet was placed in a spherical cavity of 10 nm radius using the spherical boundary condition as implemented in NAMD in order to maintain a vapor pressure equilibrium. The Newton's equation of motion for each atomic site was integrated using the velocity Verlet algorithm with a time step of 1.0 fs for the Drude oscillator modeled systems, and 2.0 fs for the nonpolarizable systems. The

Table 1: Systems and their structure characteristics using the "Drude" model. The first and second columns show the number, N, of H_2O molecules and the temperature, T of the droplet, respectively. The third and fourth columns show the equimolar radius, R_e, and the radius R_b of the bulk-like interior, respectively. The fifth column shows the number, N_i, of H_2O molecules in the droplet's bulk-like interior. In the sixth column the droplet interior density, ρ_i, is estimated from Fig. 1. In the seventh column, the droplet's pressure, P, is estimated using the Young-Laplace equation with surface tension value[94] 67 ± 4 dyn/cm for SMW4-NDP at $T = 298.15$ K. At $T = 325$ K and 350 K, P is estimated using the experimental value of surface tension, 67.5 dyn/cm and 64.0 dyn/cm, respectively. The error bars in P arise from the error bar in the surface tension. The eighth column shows the calculated bulk H_2O density, ρ_{PBC}, using MD with periodic boundary conditions (PBC). The experimental H_2O density,[107,108] ρ_{exp}, at the same conditions is shown in parentheses. By using MD with PBC we estimated the bulk density of SWM4-NDP at 300 K and $P = 1.0$ bar to be equal to 0.994 ± 0.02 g/cm^3. The error bars are one standard deviation. For comparison, Ref[109] reports density 1.0038 g/cm^3 (experimental: 0.9971 g/cm^3) at 298.15 K and $P = 1.0$ bar.

N	T (K)	R_e (nm)	R_b (nm)	N_i	ρ_i (g/cm^3)	P (bar)	ρ_{PBC} (ρ_{exp}) (g/cm^3)
200	300	1.1	0.6	31	1.028 ± 0.007	1212 ± 73	1.036 ± 0.01 (1.045)
776	300	1.75	1.1	190	1.021 ± 0.003	766 ± 45	1.022 ± 0.02 (1.028)
776	325	1.80	1.2	242	1.000 ± 0.003	771.4	1.005 ± 0.02 (1.018)
776	350	1.75	1.2	237	0.977 ± 0.004	731.4	0.982 ± 0.02 (1.004)
2000	300	2.45	1.8	830	1.015 ± 0.003	547 ± 33	1.014 ± 0.02 (1.020)
6000	300	3.55	2.9	3452	1.010 ± 0.003	378 ± 23	1.009 ± 0.02 (1.013)

duration of production runs are shown in Table S2 and Table S3 in SI, for the Drude and non-polarizable models, respectively. In the Drude model, a mass of 0.4 amu was transferred from the host atom to the Drude particle. The trajectories were visualized using VMD 1.9.4a47.[118] All the forces were computed directly without any cutoffs. For the polarizable systems, NAMD utilizes a dual Langevin thermostat to freeze the Drude oscillators while maintaining the warm degrees of freedom at the desired temperature. The systems were thermalized at 300 K for the warm degrees of freedom and at 1 K for the Drude oscillators. The damping coefficient for the Langevin thermostat was set to 1/ps.

In the analysis of the droplet structure, we used three diagnostics: (a) The mass density of H_2O, ρ, measured in spherical shells around the droplet's center of mass (COM); (b) The density arising from the Voronoi volume;[119] (c) The distance of the fifth closest neighbor to the oxygen site of water as described in Ref.[74] The Voronoi volume and the associated density were computed in the following way: The Voronoi volumes[119] for all the oxygen sites were computed. Within each spherical shell of radius r and $r + dr$ measured from the droplet's COM, the number of O sites in the shell $\mathcal{N}(r)$ and the total volume $\mathcal{V}(r)$ of the Voronoi cells for O sites was found. The average density as determined by the Voronoi cell volumes is defined as $\rho_V(r) = m\langle \mathcal{N}(r)/\mathcal{V}(r) \rangle$, where $\langle \cdots \rangle$ indicates an average over the configurations sampled in the simulations, and m is the mass of a water molecule.

In addition to the droplet simulations, bulk simulations with periodic boundary conditions (PBC) for SWM4-NDP H_2O were performed at high pressure in order to compare the radial distribution functions (RDFs) and mass density with those at the droplet's bulk-like interior.

Results and Discussion

Halide surface affinity as a function of droplet size and temperature

Figure 1 (a) and (b) show typical snapshots of a droplet with $N = 200$ and $N = 2000$, respectively, where the bulk-like interior (red), and exterior (blue), that includes the subsurface and surface are distinguished. Figure 1 (c) and (d) show three diagnostics of H_2O structure for $N = 200$ and $N = 2000$, respectively: the mass density ρ measured in spherical shells around the droplet's center of mass (COM), the denisty ρ_V using the Voronoi volume and d_5, which is the distance of the closest fifth H_2O molecule from the oxygen site of a H_2O molecule. The same diagnostics but for $N = 776$ and $N = 6000$ at $T = 300$ K, and $N = 776$ at 325 K, and 350 K are shown in Fig. S1 (a)-(d) in SI. These diagnostics vary in the same way regardless of the halide ion used. The droplet's bulk-like interior size and density extracted from those are summarized in Table 1. All the diagnostics show that the H_2O density starts to decrease at a distance R_b shown in Table 1. The decrease in density for $r > R_e$ is due to the shape fluctuations as shown in Fig. 1 (a) and (b). The density profile, ρ, masks the decrease in density due to shape fluctuations. These fluctuations become evident by using the instantenous surface[106,120–123] methods. Nevertheless, as it is discussed in the next paragraphs, the aim in this part of the study is the equilibrium constant of the ion residence time between the exterior and the droplet's bulk-like interior. This equilibrium constant does not depend on the exact definition of the surface.

One of the questions that we examine is whether the structure of the droplet interior may play a role in the location of the ions. The bulk-like interior density values, ρ_i (sixth column in Table 1), have been further examined by performing bulk simulations of SWM4-NDP with PBC under the pressure P estimated by using the Young-Laplace equation[124] at a certain R_e. The ρ_i and ρ_{PBC} values are within the standard deviation. Under the higher $P =$ 1212 bar-766 bar the RDFs of SWM4-NDP with PBC shown in Fig. 2, have a less deep first minimum than in the lower pressure. This may reflect the fact that due to the high pressure, d_5 in $N = 200$ (as shown in Fig. 1 (c)) is slightly shorter than that in the larger droplets. The small change in the H_2O coordination at this high pressure has been associated with increased H_2O fluidity.[125,126] In droplets of $N =$ 6000 where the pressure is ≈ 378 bar, the interior RDF becomes the same as that at pressure 1.0 bar. Thus, the bulk-like interior structure differs with droplet size, and this in turn may change the interplay of H_2O-H_2O and H_2O-ion enthalpies that affect the halide location. We think that at room temperature the higher pressure in the interior will not play a significant role in expelling the ions into the subsurface as shown by the fact that the bulk-like interior accommodates F^- and to some extent Cl^- in a similar manner as in the larger droplets where the pressure is lower. This argument is also supported by additional tests that are described in the next section. This is to be contrasted with the bulk-like interior in supercooled droplets from where the kosmotropic alkali and F^- may be expelled toward the subsurface. Similarly to the room temperature droplets, Cl^- can be still accommodated to some extent in the bulk-like interior of the supercooled droplets.[74]

Figure 3 (a)-(d) shows the ion number density profiles computed from the droplet's COM using the Drude model at $T = 300$ K in droplets of various sizes. Cs^+, the largest of the alkali metal ions is used here for comparison in $N = 200$ and $N = 776$. For the larger droplets, Cs^+ is expected to also reside in $r < R_b$. The raw data histograms are shown in Fig. S2 in SI and typical segments of the trajectories in Fig. S3-S6 in SI. The potentials of mean force (PMFs) along the distance of the ion from the droplet's COM for Cl^-, Br^- and I^- are shown in Fig. S7 in SI. The PMFs were computed by $-k_B T \ln(P(r))$ where k_B is the Boltzmann constant and $P(r)$ is the number density shown in Fig. 3 (a)-(d). All the number density profiles (Fig. 3 (a)-(d)), except for F^- and Cs^+, show a minimum at $\approx R_b$, which corresponds to a bar-

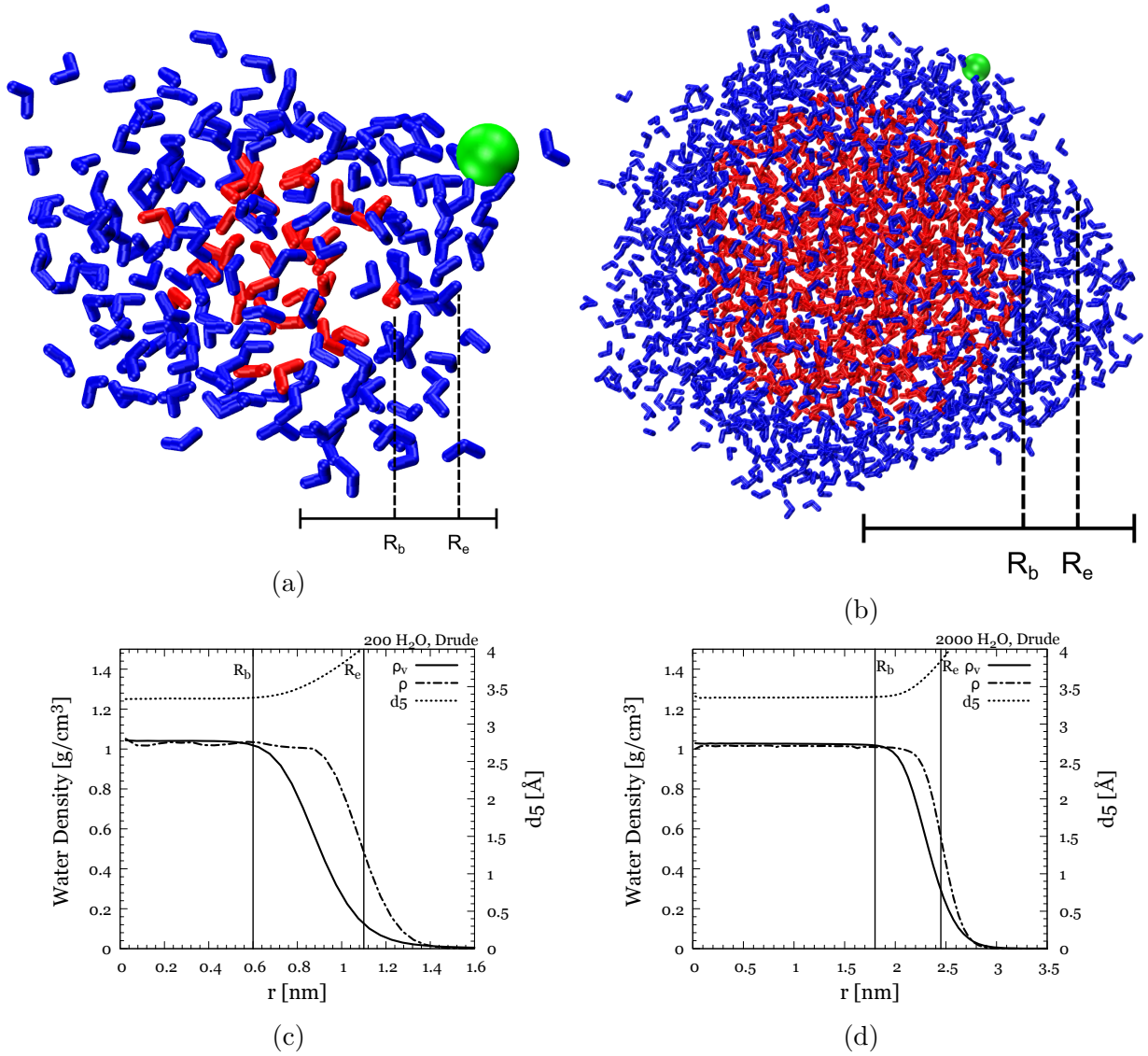

Figure 1: (a) Snapshot of $N = 200$ with a sole I^-. The red and blue colored regions show the H_2O molecules at distance, r, from the droplet's COM $< R_b$ and $r > R_b$, respectively. Beyond R_e, the shape fluctuations are observed. The I^- ion is represented by the green colored sphere, which is enlarged relative to H_2O molecules for visualization purpose. (b) Same as (a) but for $N = 2000$. (c) ρ_V, ρ, and d_5 for $N = 200$ at $T = 300$ K. (d) Same as (c) but for $N = 2000$. At $r < R_b$, ρ_V and d_5 profiles are constant before they start to decrease. Details are discussed in the text.

rier in the PMF (Fig. S7 in SI). This minimum is sharper for Br^- and I^- and slightly broader for Cl^-.

The segments of the trajectories in Fig. S3-S6 in SI show that the frequency of the incursions into the bulk like interior increase from I^- to Br^- to Cl^-. The larger the droplet, the more frequently I^- resides in $r < R_b$. In general, the larger the droplet, the longer the duration of the incursion. An incursion may last 0.4-0.5 ns in $N \leq 776$ to 1.6 ns in $N = 2000$ and $N = 6000$.

As it is already known, Br^- and I^- have a clear surface propensity relative to the other halogen and alkali ions.[4,58,62,63,67,89–92] F^- and Cs^+ have a number density that peaks at $r < R_b$, but F^- still shows a surface propensity higher than Cs^+ as shown by its decaying tail at $R_b < r < R_e$.

In previous works Cl^- has only been studied in clusters with $N < 255$, where a strong surface propensity has been found.[4,58,62,63,67,89–92] The droplet size where Cl^- can found in the in-

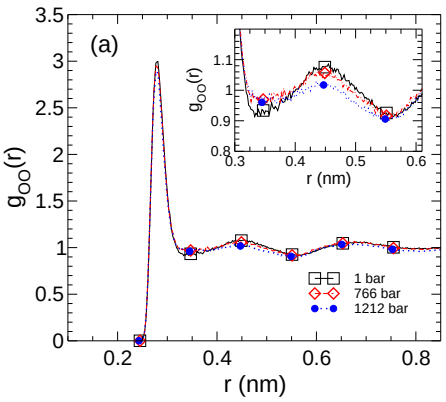

(a)

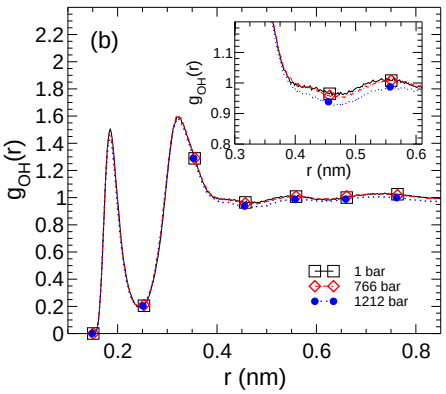

(b)

Figure 2: RDFs ($g(r)$) using the Drude model for (a) g_{OO}, and (b) g_{OH} at $P = 1$ bar and $T = 300$ K, $P = 766$ bar and $T = 300$ K, and $P = 1212$ bar and $T = 300$ K. The inset zooms in $0.3\,\text{nm} \leq r \leq 0.6\,\text{nm}$.

terior has not been reported in earlier studies. The surface propensity of Cl^- decreases with increasing droplet size, and in the largest droplets of $R_e = 3.55$ nm, the interior location of Cl^- is favored relative to the exterior.

Table 2 shows the ion's percentage residence time in the exterior. Using these data, we compute the equilibrium constant of the exterior over interior residence time shown in Table 3. The probability to encounter the ion into the bulk-like interior depends on the volume. To do a democractic comparison, we compare, within the same droplet size, the ratio of the percentage residence time shown in Table 2, among Cl^-, Br^- and I^- at $r > R_b$. We find that the $[Cl^-]/[I^-]$ ratio decreases from 0.92 in $N = 200$ to 0.72 in $N = 2000$. In $N = 6000$ this ratio decreases considerably to 0.53. The $[Cl^-]/[Br^-]$ ratio also decreases from 0.93 in $N = 200$ to 0.75 in $N = 2000$.

The difference in the $\Delta\Delta A$ between the exterior and bulk-like interior for certain droplet sizes modeled by SWM4-NDP is reported in Table 4. The free energy difference decreases with the droplet size, which implies that the interplay of the molecular factors that determine the ion location may change with the size.

Table S4 in SI shows the integrated number density of the ions at $r > R_b$. In Ref.[92] a H_2O-ion model very near to the Drude is used to compute the free energy differences as a function the ion-droplet COM distance for $N \approx 200$. In Ref.[92] the interior is defined in the interval (0,7.5 Å) and the exterior (surface and subsurface) is defined in the interval (7.5 Å,11 Å), while in our study for approximately the same system size we use the value of 6.0 Å, which is the minimum of the number density profiles (maximum in the PMF in Fig. S7 in SI). We note that we define the equilibrium constant (Table 3) differently from that in Ref.[92] If we estimate the equilibrium constant as in Ref.[92] taking as the droplet exterior $r > 7.5\text{Å}$, then $K_{\text{eq}}^{\text{X}} = 2.02$, 8.9 and 14.4 for Cl^-, Br^-, I^-, respectively, which compares reasonably well with the values 1.6, 7.0 and 13.0 reported in Ref.[92] In Ref.[92] comparison of the equilibrium constant for $N \approx 200$ are made with X-ray photoelectron spectroscopy (XPS) experiments for planar interfaces. We think that it may not be obvious a priori that the planar interface ion distribution will be comparable with the ion distribution in $N = 200$. A droplet with $N = 200$ differs from the larger droplets in the thickness of the interfacial region, which includes the subsurface and surface[127] where $|R_e - R_b|$ equals 0.5 nm for $N = 200$ vs 0.65 nm for the larger clusters. In $N = 200$, the ions are nearer the bulk-like interior and the peaks of I^- and Cl^- are nearer to one another than in the larger droplets. Specifically, the distance of the maximum of the Cl^- number density from R_b is 2.8 Å in $N = 200$, and converges to the value of 4.5 Å in the larger droplets. Similarly, the distance between the

Table 2: Percentage of ion residence time in the exterior of the droplet (Δt_{ext} (%)) for X^- = F^-, Cl^-, Br^-, I^- in various models at $T = 300$ K. The dividing surface between interior and exterior is $r = R_b$. R_b is defined at 6 Å, 11 Å, 18 Å, 29 Å for $N = 200$, 776, 2000 and 6000, respectively. The dash lines in the Table indicate that simulations have not been performed for these systems. The long simulation time in the larger systems prevents us to perform simulations of Br^- in $N = 6000$ and F^- in $N = 2000$ and $N = 6000$. It is expected that F^- will be found in the interior even for $N = 2000$ and $N = 6000$.

Model	N	Δt_{ext} (%), F^-	Δt_{ext} (%), Cl^-	Δt_{ext} (%), Br^-	Δt_{ext} (%), I^-
Drude	200	52.3 ± 1.9	91.4 ± 1.3	98.7 ± 0.5	99.6 ± 0.3
	776	49.5 ± 3.6	81.8 ± 1.4	95.7 ± 1.7	99.0 ± 0.5
	2000	–	67.9 ± 1.5	90.3 ± 3.4	94.9 ± 1.7
	6000	–	46.6 ± 4.1	–	86.4 ± 8.4
OPLS	776	39.1 ± 1.0	46.5 ± 1.7	48.7 ± 0.9	64.5 ± 1.3
OPLS‡	776	48.2 ± 0.5	80.5 ± 1.1	88.1 ± 0.6	99.4 ± 0.2
M19	776	53.0 ± 0.6	67.7 ± 1.0	74.9 ± 0.8	88.7 ± 0.9

Table 3: Equilibrium constant K_{eq}^X (X = F, Cl, Br, I) computed by the ratio of the ion residence time at the exterior ($r > R_b$) over the interior region. The boundary between the exterior and the interior is defined at R_b shown in Table 1. The dash lines in the Table indicate that simulations have not been performed for these systems because the outcome is expected. Details are discussed in the text.

Model	N	K_{eq}^F	K_{eq}^{Cl}	K_{eq}^{Br}	K_{eq}^I
Drude	200	1.1 ±0.08	10.6 ±2.3	75.9 ±29	249
	776	0.98 ±0.14	4.4 ±0.4	22.3 ±9.2	99
	2000	–	2.1 ±0.2	9.3 ±3.6	18.6 ±6.5
	6000	–	0.83 ±0.2	–	6.1 ±4.5
OPLS	776	0.64 ±0.03	0.87 ±0.06	0.3 ±0.03	1.9 ±0.06
OPLS‡	776	0.93 ±0.02	4.1 ±0.3	7.4 ±0.12	166 ±55
M19	776	1.13 ±0.03	2.1 ±0.1	3.0 ±0.13	7.8 ±0.7

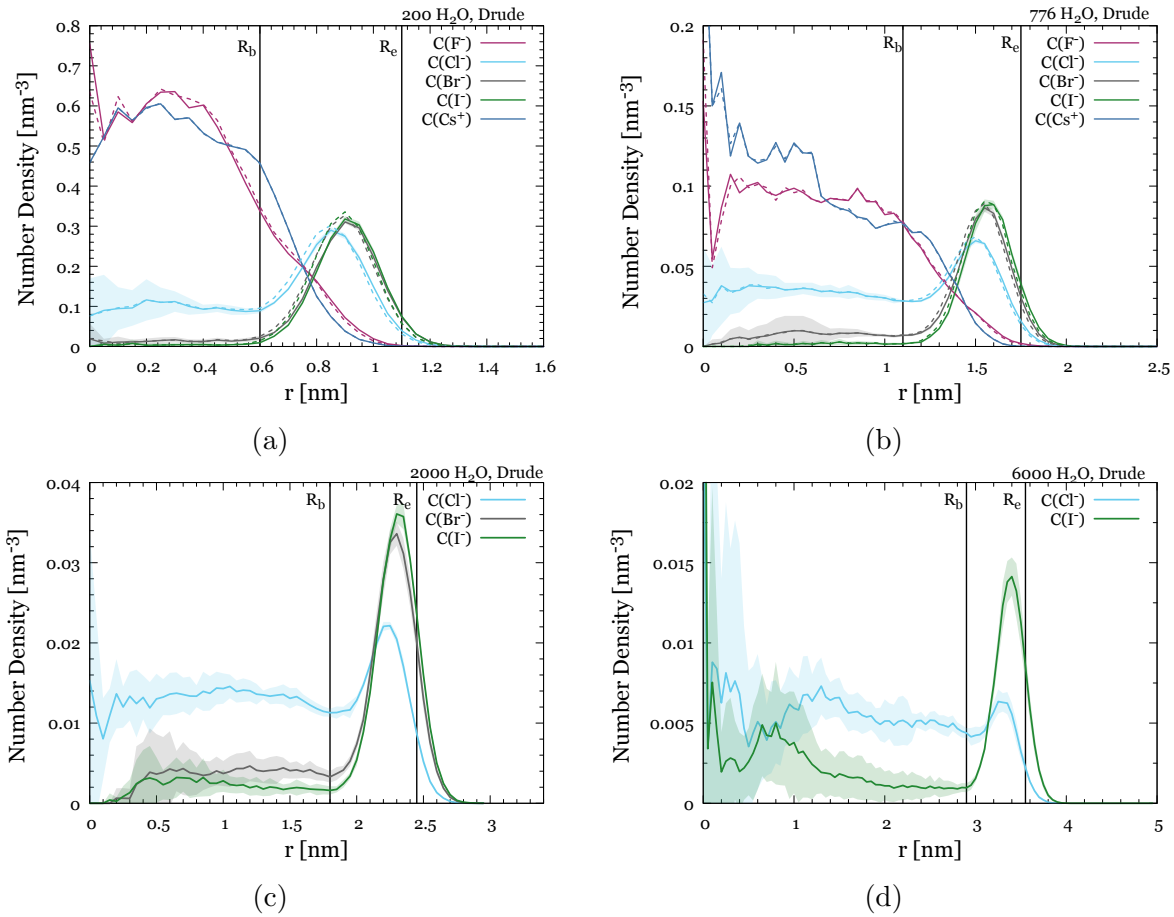

Figure 3: Number density profiles in units of concentration measured from the droplet's center of mass (COM) of an embedded sole ion in an aqueous system comprised (a) $N = 200$, (b) $N = 776$, (c) $N = 2000$, and (d) $N = 6000$. R_b and R_e mark the bulk radius and the equimolar radius, respectively. In (a) and (b), the location of the Drude particle is shown in dotted lines. Standard deviation obtained by block averaging over five equally spaced blocks is shown for Cl^- only in (a) - (d) and also for I^- in (d). The standard deviations for the other ions are of the same magnitude as for Cl^-. The bin size used is 0.5 Å. Simulation length of the systems is shown in Table S3 in SI. The histogram of the ion distance from the COM using the raw data are shown in Fig. S2 in SI.

Table 4: $\Delta\Delta A$ (kJ/mol) for F^-, Cl^-, Br^-, and I^- using the K_{eq}^X from Table 3 for SWM4-NDP.

N	F^-	Cl^-	Br^-	I^-
200	−0.23	−5.9	−10.8	−13.8
776	0.05	−3.8	−7.7	−11.5
2000		−1.9	−5.6	−7.3
6000		0.48	− − −	−4.5

Cl^- and I^- number density maxima increases from 0.4 Å in $N = 200$ to 1.0 Å in the larger droplets. At $N \approx 776$ there is a convergence in the thickness of the surface and subsurface region and in the location of the exterior maxima of the ion number density profiles.

We compare the number density of the single ion with the ion distributions in a planar interface. The half thickness of the planar interface that is simulated in Ref.[21,40] is ≈ 1.75 nm. This thickness includes the shape fluctuations. In the droplets studied here, R_e ranges between 1.10 nm ($N = 200$) to 3.55 nm ($N = 6000$). The linear dimension of the droplet is longer than R_e by ≈ 4 Å when shape fluctuations are

included. Thus, a droplet of $N \approx 800-900$ H_2O is nearer a $3\times3\times3$ nm^3 slab simulated with periodic boundary conditions (PBC) in Ref.[21,40] In the planar interface,[21,40] there is a high concentration of ion pairs (1.0 M-1.2 M) and overall the interface is neutral. The location of Na^+ and X^- may be correlated because of ion pairing, a factor that might also affect the ion depth distribution. Comparison with Figure 10 in Ref.[21] shows that overall, there are similarities in the trend of the halide location between a planar interface and a $N \gtrapprox 776$ nanodroplet. We note that in our simulations for Cl^- and I^- it is the nanodroplets with $N = 2000$ that start to show a similar trend to the planar interface (Fig. 10 in Ref.[21]) by showing a maximum in the bulk-like interior. It is noted that the distance between the number density maxima in the interior and surface for Cl^- and I^- are at a much longer distance in the $N = 6000$ nanodroplet relative to the slab. For instance, the distance for I^- is 28 Å relative to the slab that it is 13 Å. Possibly the difference arises from the finite thickness of the slab.

The temperature effect in the number density profiles of the ions is shown in Fig. 4. All the polarizable halides gradually lose their surface affinity with the temperature increase. Cl^- completely loses its surface affinity at 350 K, while I^- and Br^- still keep some surface preference. The shift of the ion number density toward the bulk interior may be attributed to decreased strength of interaction between the polarized surface and the ion due to increased thermal motion that in turn reduces the degree of the surface orientation of the H_2O molecules. The surface and ion polarization are discussed in the next section. There may be other factors that also contribute in the loss of the surface preference such as easier accommodation of the larger ions in the interior because of more labile H-bonding and higher dielectric constant in the interior that leads to better solvation.

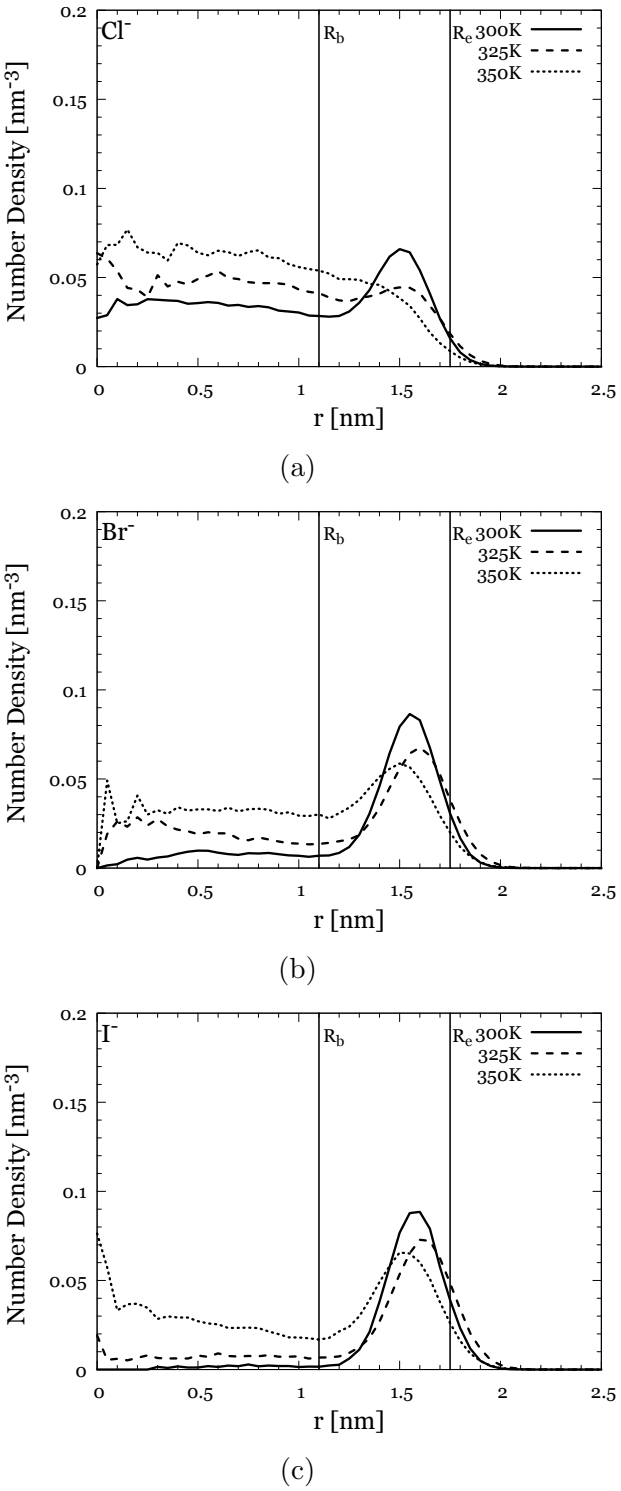

Figure 4: Ion number density profile of a droplet comprised 776 H_2O molecules and a sole ion (a) Cl^-, (b) Br^-, (c) I^- at 300 K, 325 K and 350 K.

Factors that affect the surface affinity of halide ions

Several works have analyzed the factors that determine the ion location, by estimating the

relative size of H_2O-H_2O and H_2O-ion enthalpies[62,63,89,92] (ΔH) for clusters with $N \lessapprox 200$. In Ref.,[92] for $N \approx 200$, the enthalpic contribution arising from the sum of the H_2O-H_2O and H_2O-ion average potential energies were estimated[92] by constraining the ion's position along the distance from the droplet's COM. It was found[92] that ΔH (difference between the exterior enthalpy and the interior) ranges from ≈ -30 kJ/mol for I^- to ≈ -5 kJ/mol for F^-. Entropic contributions were computed[92] by subtracting the enthalpic contributions from the computed PMF profiles. It was found[92] that in $N \approx 200$, F^- resides in the interior because of a dominant entropic contribution while the other halides reside near the surface because of a dominant enthalpic contribution. We think that by computing the H_2O-H_2O and H_2O-ion average potential energies we cannot clearly determine whether the strength of the water network prevents the ions entering the cluster interior especially in smaller ($N \lessapprox 800$) clusters. The reason for that is that the presence of the ion in the bulk-like interior in $N = 200$ affects the entire H_2O interior network since the ion's second hydration shell extends up to near 6.0 Å for the various ions (Fig. S8 in SI), which is almost equal to R_b (Table 1). Even in $N = 776$ the effect of the ion in the structure of the bulk-like interior ($R_b = 1.1$ nm) is still considerable. Moreover, near the interface, the constraint of the ion-COM distance may influence the droplet's shape fluctuations and thus, the PMF near the interface. An order parameter that monitors the distance of the ion from the instantenous interface, may provide a more representative picture of the ion location.[106,120–123]

One way to examine the average depth of the ions from the surface is to examine the RDFs of the ions in the bulk-like interior vs those in the exterior as shown in Fig. S8 in SI for halide ions in the Drude model. For example the solvation of I^- is reduced by ≈ 2.5 H_2O molecules when it is on the surface, which shows partial exposure to the interface.

Another approach to assess the factors that determine the ion location is to consider the H_2O-H_2O and H_2O-ion interactions collectively as they give rise to the following thermodynamic factors:[45,100,102] (a) The hydrophobic effect that arises from the ion size. This effect leads to a free energy penalty to create a cavity within the H_2O network. (b) The ion solvation due to charge and its sign. An ion in the interface may be partially solvated, which leads to a free energy penalty relative to the completely solvated state. (c) The interaction of the ion with the surface potential.[28,103–106] The factors that determine the ion location are often inferred via comparison of different force fields and via assessing the effect of certain interactions within the force field by nullifying their contributions. Since all the model parameters are intertwined we cannot universally deduce the factors that determine the ion location by systematically switching-off the values of certain parameters. These tests may reveal the factors that affect the ion location within the particular molecular model, which may not be transferable to other models or to reality.

We examine whether the interaction of the ion with the surface potential is the main driving force that determines the location of the polarizable halides near the surface. The surface potential also includes the effect of the H_2O polarization due to the presence of the ion. For SWM4-DP planar interface the vapour/water surface potential has been estimated[28,94,128] to be -545 mV. It is noted here that the surface potential found in ab initio simulations[103–105] and experiments[104,129] has a different sign from that of the classical force fields. This sign difference has been explained[28,130] as originating from the difference in the water quadrupolar tensor trace. It has also been found that the orientation of the interfacial water in both ab initio and classical force fields is in agreement.[28]

The radial dipole moment was calculated by projecting the dipole moment of a molecule onto the vector from the center of mass of the droplet to the center of mass of the molecule. The radial distribution of the projected component ($p_r(r)$) was calculated by averaging over all molecules found within a spherical shell with radius r and $r + dr$ and over all the configurations. For water molecules, the induced dipole moment arises from both the orientation of the H_2O molecules and the electronic polarization

represented by the Drude oscillator. Here, we use the convention where the dipole moment points from negative to positive charge sites, therefore a positive $p_r(r)$ value represents an excess positive charge in the region due to polarization, caused by the interface and the ion.

To analyze the polarization of the ion we discuss Fig. 5 in relation to the histogram of the raw data of the ion location, shown in Fig. S3 in SI. Fig. 5 shows a strong halide polarization in $R_b < r < R_e$ relative to the interior for $N = 200$ and $N = 776$ at $T = 300$ K-350 K. The degree of polarization decreases with increasing droplet size or temperature. Overall, the ion polarization follows the expected trend for the halides. In $N = 200$ the ion polarization starts at $r < R_b$ because of the droplet's shorter $|R_e - R_b|$ interval relative to $N \gtrapprox 776$. In Fig. S3 in SI the raw data in the histogram for F^- and Cl^- show that F^- has a significant presence in $R_b < r < R_e$. F^- and Cl^- are found in the subsurface, where they are still well solvated. Thus, their polarization has to be induced by the orientation and electronic polarization of the H_2O molecules in the surface and subsurface region. For Br^- and I^-, the asymmetric solvation[90,131] due to their partial exposure toward the vapour may lead to enhanced polarization.

Figure 6 shows the averaged radially projected water dipole moment. The projection shows that the H_2O polarization decreases with increasing droplet size and temperature. The polarization effect is more pronounced in droplets with $N \approx 200$, where the type of the ion will affect the degree of H_2O polarization. It is noted that the H_2O polarization is caused not only by the orientation due to the interface but also by the presence of the ion itself. In $N = 200$ the effect of the ion in the surrounding H_2O is more pronounced, where F^- shows the largest effect. The H_2O polarization is also reflected in the charge distribution around the droplet's COM shown in Fig. S9 and Fig. S10 in SI. Thus, for $N \lessapprox 776$ the relative strength of ion-H_2O and H_2O-H_2O interactions as a function of the distance from the droplet's COM may change. The ion polarization is caused by the polarization of the exterior H_2O, since the H_2O in the bulk-like interior do not cause

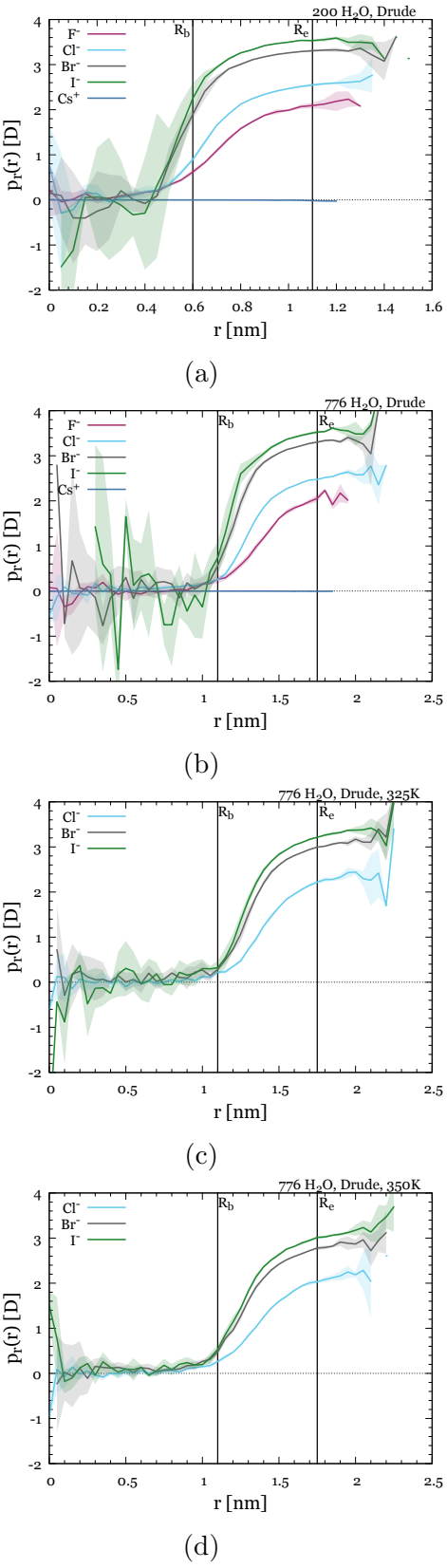

Figure 5: Time-averaged radial dipole moment (p_r) of the ion as a function of its radial position for (a) $N = 200$ at $T = 300$ K, (b) $N = 776$ at $T = 300$ K, (c) $N = 776$ at $T = 325$ K, and (d) $N = 776$ at $T = 350$ K.

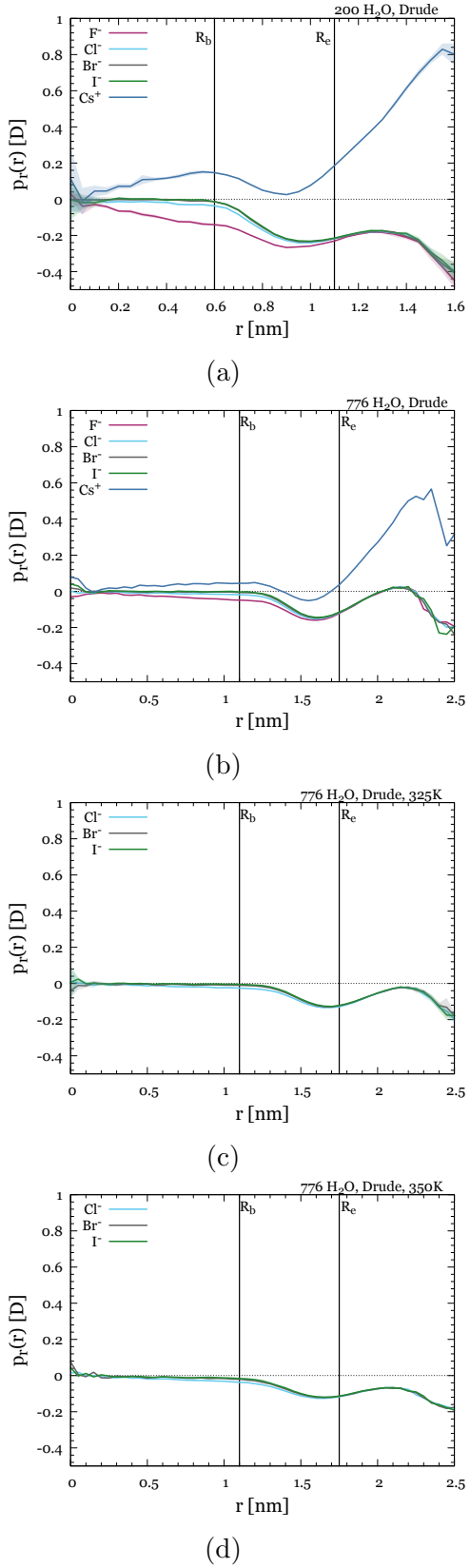

Figure 6: Same as Fig. 5 but for the water molecules.

any significant polarization except for $N = 200$. Our analysis so far supports the existence of the interaction of the polarized halide with the surface potential, but they cannot clearly show that this interaction is the driving force for the presence of the halides on the surface. Supporting evidence of the key role of this interaction in determining the ion position comes from simulations of a sole Cl^- in $N = 200$ using the SWM4-NDP model where the Cl^- polarization was nullified and all the other parameters were kept the same. Figure S11 in SI shows that Cl^- for $N = 776$ and $T = 300$ K loses its surface affinity and resides in the droplet's interior. This suggests that the polarizable Cl^- is captured in the interface due to the surface potential. As we will discuss in the next paragraphs, I^- already shows a degree of surface affinity in TIP4P/2005, thus, it is expected that polarization will enhance its surface propensity. Our results for the role of the surface potential is along the explanation for the preference of the polarizable halides in the planar interface.[131] The difference in the droplets is that there is a size effect on the degree of the ion-interface interaction.

We draw further insight about the factors that determine the ion location by examining the number density profiles of halides in TIP4P/2005 with ions that carry charge -1 and in charge-scaled force fields that intend to treat the ion polarization in an average manner, shown in Fig. 7. The ion-oxygen site radial distribution functions (RDFs) for the various force fields are shown in Fig. S12 in SI and the hydration numbers of the ions are shown in Table S5 in SI. OPLS (which in our notation denotes the use of TIP4P/2005 for H_2O and ion charge -1) for $N = 776$ predicts the maximum of the F^- number density profile near the droplet's COM, in agreement with SWM4-NDP. Using the same model, Cl^- and Br^- show a smoothly increasing number density toward the droplet's COM, but not as sharp as that of F^-. Cl^- and Br^- show a small degree of propensity at $R_b < r < R_e$. I^- shows a slight increase towards the COM and it clearly shows a local maximum at $R_b < r < R_e$. Thus, even though OPLS does not explicitly treat the solvent and ion polarization, it still

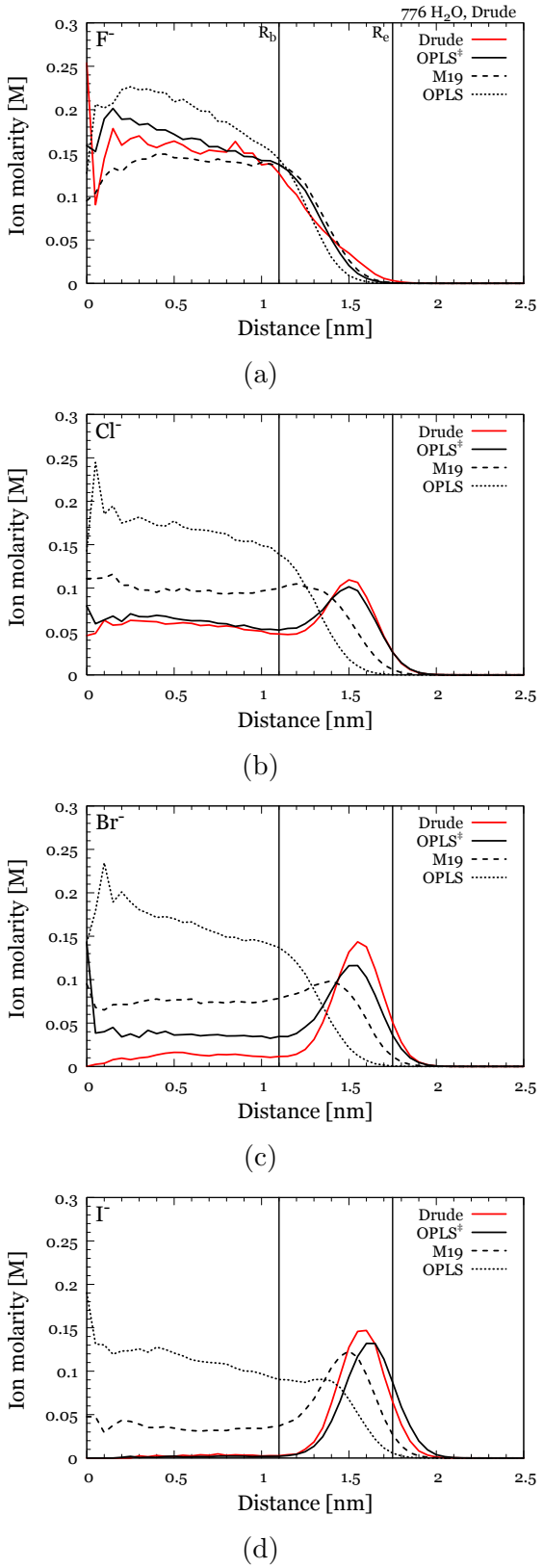

Figure 7: Number density profiles at $T = 300$ K for $N = 776$ and a single halide ion using different models. (a) F^-; (b) Cl^-; (c) Br^-; (d) I^-.

predicts a trend in the number density profiles consistent with the halides increasing polarizability from F^- to I^-. As it was discussed in the previous paragraph, electronic polarization enhances this trend. The orientation of the H_2O molecules around the ion may affect its interaction with the surface potential, which is appears to be the driving force for determining the halide location in the OPLS.

Figure 7 shows that in the OPLS‡ (where H_2O is modeled by TIP4P/2005) a decrease of the ion charge[89] at -0.75, predicts number density profiles near that of Drude model (where H_2O is modeled by SWM4-NDP). The hydrophobic effect is the same as in the OPLS model. The fact that the $F^{0.75-}$ appears in the interior indicates that the weaker ion-H_2O interactions and the high interior pressure of the droplet do not prevent the ion to be found mainly in the interior. Thus, the reduced need for solvation for $Cl^{0.75-}$, $Br^{0.75-}$ and $I^{0.75-}$ creates a new favorable location relative to OPLS where the combination of the hydrophobic effect, solvation and interaction with the surface potential lead to lower energy.

The number density profiles for $N = 776$ using the M19 model (where H_2O is modeled by TIP4P/2005 and the ion Lennard-Jones parameters are different from those in OPLS and OPLS‡), shown in Fig. 7, predict a similar trend to Drude but less pronounced. The M19 model intends to reproduce the structure of aqueous solutions and results in a concentration profile that resembles that of multiple ions in solution between the ion and water in the surface and subsurface.

In order to determine the role of the combination of charge sign and size we simulated $N = 776$ and a sole Cl^+, Br^+ and I^+ using SWM4-NDP and OPLS‡ and $N = 200$ using SWM4-NDP. The use of halides with a positive charge has a physical meaning. All alkali ions and F^- are classified as hard ions, Cl^- is in the borderline, and Br^- and I^- are classified as soft ions. Quantum ab initio calculation have shown that F^+, Cl^+, Br^+ and I^+ have comparable, but slightly higher hardness to their anionic counterparts as they have similar ionic radius.[132,133] The number density profiles using SWM4-NDP

and OPLS‡ are shown in Fig. S13 (a)-(b) and (c), respectively. Figure S13 (a)-(b) for SWM4-NDP shows that X^+ does not have a surface propensity for $N = 200$ and $N = 776$, which agrees with previous studies.[92] The X^+ number density is higher in the region where the Voronoi volume computed density has a steady value (bulk-like interior), and the droplet interior is explored in a uniform manner. This indicates that the high density bulk interior does not prevent the formation of a cavity to enclose an ion of the size of I^-. The number density profiles suggest that the solvation of the X^+ and repulsion from the interface dominate in placing the ions in the bulk-like interior. The fact that the alkali ions and positively charged halides prefer the interior in polarizable and non-polarizable models shows that the charge sign leads to different solvation from that of the large anions and repulsion from the interface. These findings are in line with those in Ref.[56]

Figure S13 (c) in SI shows that in OPLS‡ the positively charged counterpart of halides with charge +0.75 also show surface propensity. The modification in OPLS‡ is in the decreased ion charge, which decreases the strength of ion-H_2O interactions, leading to a surface propensity of positively charged halides as well. The ± 0.75 scaled-charged ions in OPLS‡ if they interact with the surface potential, they will have an opposite interaction. Thus, the effect of the interactions of the ions with the surface potential is not the reason for the ion location. The similarity in the surface propensity between $X^{0.75-}$ and $X^{0.75+}$ suggests that it is due to the hydrophobic effect and due to the strength of the H_2O-H_2O interactions that prevents their disruption by the ion of the low charge.

The tests lead to the following conclusions: (a) For the halide ions, the strength of the H_2O-H_2O interactions in the bulk-like interior of the droplet is not the decisive factor that prevents the ions to be found in this region. Thus, the hydrophobic effect does not play a key role for the halides. (b) Simulations provide evidence that the surface potential is the driving force for the location of Cl^-, Br^-, I^- nearer the droplet surface in the Drude model. Simulations also suggest that the surface potential induces a dipole moment to the large polarizable halides that stabilizes their surface location in agreement with previous studies.[90,131] (c) In $N \lessapprox 776$ the H_2O polarization is more obviously affected by the strong orientation of the H_2O molecules in the first hydration shell of the ion. (d) In non-polarizable models such as TIP4P/2005 the ion number density profiles show a similar trend to that of the polarizable force field but less pronounced. The reduced charge density of halide ions, using charge-scaling may lead to number density profiles similar to those of a polarizable force field. Thus, different interplay of interactions in a force field may lead to number density profiles similar to those of a polarizable force field (considering the polarizable force field as a reference model). Thus, nullifying parameters in a force fields in order the understand the physical factors that determine the ion location, does not provide transferable insight to other force fields or reality.

Conclusion

By using the polarizable model SMW4-NDP we showed that the surface propensity of the polarizable halides (Cl^-, Br^-, I^-) decreases by increasing the droplet size or temperature. At $T = 300$ K and in an aqueous droplet with an equimolar radius of ≈ 1.1 nm ($N \approx 200$ H_2O), which is the smallest size examined in this study, these halides show the largest surface propensity relative to larger ones. The increase of droplet size or temperature affects mostly the surface propensity of Cl^-. In droplets with equimolar radius ≈ 3.55 nm ($N \approx 6000$ H_2O) at $T = 300$ K Cl^- is mainly located in the bulk-like droplet interior. I^- preserves a degree of surface propensity even in the larger droplets, and, it also shows a significant maximum in the bulk-like interior. From the smallest droplets, $N = 200$ that we studied to the largest, $N = 6000$, the relative (measured from the bulk solvation energy) interfacial free energy increases by ≈ 6.3 kJ/mol for Cl^-, and ≈ 9.3 kJ/mol for I^-. Overall, the relative interfacial free energy is of the order of magnitude of several kJ/mol for all the halides. At

elevated temperatures the surface propensity of Cl^- decreases gradually, and at $T = 350$ K, Cl^- loses the distinct maximum of its number density profile at the droplets' exterior. I^- still preserves its surface propensity at $T = 350$ K but to a lesser degree than at $T = 300$ K. The number density profiles of the polarizable halides starting from $N = 2000$ and at $T = 300$ K show a maximum in the interior in addition to the surface as those in the simulated aqueous planar interface at $T = 300$ K. The convergence toward the planar interface shows that even in the smaller nanodroplets, same forces, namely the interaction of the polarizable halide with the surface potential, to those in a planar interface determine the ion location. Still certain differences exist between droplets of $N = 2000-6000$ and the planar interface in the distance of the number density maxima between the surface and bulk-like interior. We attribute this difference in the finite thickness of the planar interface.

We assessed three charge-scaled nonpolarizable force-fields in predicting the halide surface propensity by using a Drude oscillator-based polarizable model as a reference model. We found that TIP4P/2005, even though does not explicitly treat the solvent and ion polarization, it still predicts a trend in the number density profiles consistent with the halides' increasing polarizability from F^- to I^-. We attribute this trend to the interaction of the halide ions with the surface potential. A number of tests by changing the charge sign, magnitude, and polarizability showed that the interaction between the polarizable halide and the surface potential plays a key role in determining the location of the polarizable halides. We also showed that different driving forces in force fields may lead to number density profiles for the ions that are similar to those of the polarizable force field that we use as reference model. Thus, nullifying parameters in a force fields in order the understand the physical factors that determine the ion location, does not provide transferable insight to other force fields.

Since we found that clusters with several thousands of H_2O provide ion density profiles similar to those of a planar interface, liquid-jet experiments using XPS at elevated temperatures may confirm the temperature effect in the ion distributions in planar interfaces.[18,34] This result will be also transferable to larger clusters. The effect of temperature in the location of halides is expected to have profound consequences in the photochemistry of atmospheric aerosols.[5,6] New applications of crossed molecular beam experiments in aerosol nanoclusters[134] combined with electrospray ionization for selecting cluster sizes may provide information on the growth mechanisms of the clusters depending on the nature of the ion. In these experiments clusters comprised several thousands of solvent molecules are accessible.

The location of the ions is also expected to have implications in nucleation of supersaturated vapor.[13,135] The presence of the ions lowers the nucleation barrier relative to pure H_2O and decreases the size of the critical nuclei. Depending on temperature and degree of supersaturation the critical nuclei are expected to contain only a few tens of H_2O molecules at most. Because of the small size there is no distinction between interior and exterior location, thus it is expected that the classical nucleation theory that is based on the division of surface and volume contributions may need to be revised. The interior and exterior ion states are expected to manifest in the larger post-critical clusters. Nucleation processes upon cooling within the larger droplets where the ion may serve as a nucleation center may be also affected by the ion location.

Supporting Information

(S1.) System and simulation parameters; (S2.) Water structure in droplets using the Drude model; (S3.) Raw data of the ion distribution and trajectories in Drude-modeled droplets; (S4.) Potential of mean force as a function of the ion-droplet's COM distance; (S5.) Residence time of the ion in the exterior divided by the volume; (S6.) Ion-Oxygen RDFs in the droplet's bulk-like interior and exterior; (S7.) Charge density profiles; (S8.) Cl^- number density profile in SWM4-NDP H_2O by removing

the Cl^- polarization; (S9.) Comparison of the radial distribution functions of Ion-Oxygen for various molecular models; (S10.) Number density profiles for X^+ in aqueous droplets.

Acknowledgments

S.C. expresses gratitude to Prof. J. C. Hemminger, and Prof. D. Tobias, Department of Chemistry, University of California, Irvine for sharing their knowledge on the ion distributions in planar interfaces, to Prof. D. Frenkel, Yusuf Hamied Department of Chemistry, University of Cambridge, UK, Prof. R. Kapral, Department of Chemistry, University of Toronto, Prof. B. J. Finlayson-Pitts as well as the group members, Dr. Lisa M. Wingen, and Dr. Veronique Perraud in the Department of Chemistry, University of California at Irvine, Prof. S. S. Xantheas, Pacific Northwest National Laboratory, Prof. Ivan Saika-Voivod, Department of Physics and Physical Oceanography, Memorial University of Newfoundland, and Dr. Anatoly Malevanets for insightful discussions on ion-cluster interactions. S.C. acknowledges an NSERC-Discovery grant (Canada) for funding this research. V.K. acknowledges the Province of Ontario and the University of Western Ontario for the Queen Elizabeth II Graduate Scholarship in Science and Technology. Digital Research Alliance of Canada is acknowledged for providing the computing facilities.

References

(1) Tong, Y.; Zhang, I. Y.; Campen, R. K. Experimentally quantifying anion polarizability at the air/water interface. *Nat. Commun.* **2018**, *9*, 1313.

(2) Vaida, V. Perspective: Water cluster mediated atmospheric chemistry. *J. Chem. Phys.* **2011**, *135*, 020901.

(3) Ruiz-Lopez, M. F.; Francisco, J. S.; Martins-Costa, M. T.; Anglada, J. M. Molecular reactions at aqueous interfaces. *Nat. Rev. Chem.* **2020**, *4*, 459–475.

(4) Petersen, P. B.; Saykally, R. J. On the nature of ions at the liquid water surface. *Annu. Rev. Phys. Chem.* **2006**, *57*, 333–364.

(5) Knipping, E.; Lakin, M.; Foster, K.; Jungwirth, P.; Tobias, D.; Gerber, R.; Dabdub, D.; Finlayson-Pitts, B. Experiments and simulations of ion-enhanced interfacial chemistry on aqueous NaCl aerosols. *Science* **2000**, *288*, 301–306.

(6) Gerber, R. B.; Varner, M. E.; Hammerich, A. D.; Riikonen, S.; Murdachaew, G.; Shemesh, D.; Finlayson-Pitts, B. J. Computational studies of atmospherically-relevant chemical reactions in water clusters and on liquid water and ice surfaces. *Acc. Chem. Res.* **2015**, *48*, 399–406.

(7) Rogers, M. M.; Vazquez de Vasquez, M. G.; Neal, J. F.; Zerkle, M. M.; Shook, B. M.; Allen, H. C. Phase State and Thermodynamic Properties of Proxy Sea Spray Aerosol Interfaces Derived from Temperature-Dependent Equilibrium Spreading Pressure. *ACS Earth and Space Chemistry* **2022**, *6*, 1563–1573.

(8) Cheng, J.; Vecitis, C. D.; Hoffmann, M.; Colussi, A. Experimental anion affinities for the air/water interface. *J. Phys. Chem. B* **2006**, *110*, 25598–25602.

(9) Narayan, S.; Muldoon, J.; Finn, M.; Fokin, V. V.; Kolb, H. C.; Sharpless, K. B. "On water": unique reactivity of organic compounds in aqueous suspension. *Angewandte Chemie* **2005**, *117*, 3339–3343.

(10) Jung, Y.; Marcus, R. On the theory of organic catalysis "on water". *J. Am. Chem. Soc.* **2007**, *129*, 5492–5502.

(11) Kahan, T.; Kwamena, N.-O.; Donaldson, D. Different photolysis kinetics at the surface of frozen freshwater vs. frozen salt solutions. *Atmospheric Chem. Phys.* **2010**, *10*, 10917–10922.

(12) Zhong, J.; Kumar, M.; Anglada, J.; Martins-Costa, M.; Ruiz-Lopez, M.; Zeng, X. C.; Francisco, J. S. Atmospheric Spectroscopy and Photochemistry at Environmental Water Interfaces. *Annu. Rev. Phys.* **2019**, *70*, 45–69.

(13) Oh, K.; Gao, G.; Zeng, X. C. Nucleation of water and methanol droplets on cations and anions: the sign preference. *Phys. Rev. Lett.* **2001**, *86*, 5080.

(14) Davis, R. D.; Tolbert, M. A. Crystal nucleation initiated by transient ion-surface interactions at aerosol interfaces. *Sci. Adv.* **2017**, *3*, e1700425.

(15) Olivieri, G.; Parry, K. M.; D'Auria, R.; Tobias, D. J.; Brown, M. A. Specific anion effects on Na+ adsorption at the aqueous solution–air interface: MD simulations, SESSA calculations, and photoelectron spectroscopy experiments. *J. Phys. Chem. B* **2018**, *122*, 910–918.

(16) Ben-Amotz, D. Interfacial solvation thermodynamics. *Journal of Physics: Condensed Matter* **2016**, *28*, 414013.

(17) Tobias, D. J.; Stern, A. C.; Baer, M. D.; Levin, Y.; Mundy, C. J. Simulation and theory of ions at atmospherically relevant aqueous liquid-air interfaces. *Annu. Rev. Phys. Chem.* **2013**, *64*, 339–359.

(18) Ghosal, S.; Hemminger, J. C.; Bluhm, H.; Mun, B. S.; Hebenstreit, E. L.; Ketteler, G.; Ogletree, D. F.; Requejo, F. G.; Salmeron, M. Electron spectroscopy of aqueous solution interfaces reveals surface enhancement of halides. *Science* **2005**, *307*, 563–566.

(19) Jungwirth, P.; Tobias, D. J. Surface effects on aqueous ionic solvation: A molecular dynamics simulation study of NaCl at the air/water interface from infinite dilution to saturation. *J. Phys. Chem. B* **2000**, *104*, 7702–7706.

(20) Wang, L.; Morita, A.; North, N. M.; Baumler, S. M.; Springfield, E. W.; Allen, H. C. Identification of Ion Pairs in Aqueous NaCl and KCl Solutions in Combination with Raman Spectroscopy, Molecular Dynamics, and Quantum Chemical Calculations. *J. Phys. Chem. B* **2023**, *127*, 1618–1627.

(21) Jungwirth, P.; Tobias, D. J. Specific ion effects at the air/water interface. *Chemical reviews* **2006**, *106*, 1259–1281.

(22) Horinek, D.; Herz, A.; Vrbka, L.; Sedlmeier, F.; Mamatkulov, S. I.; Netz, R. R. Specific ion adsorption at the air/water interface: The role of hydrophobic solvation. *Chem. Phys. Lett.* **2009**, *479*, 173–183.

(23) Psillakis, E.; Cheng, J.; Hoffmann, M.; Colussi, A. Enrichment factors of perfluoroalkyl oxoanions at the air/water interface. *J. Phys. Chem. A* **2009**, *113*, 8826–8829.

(24) Cheng, J.; Hoffmann, M. R.; Colussi, A. Anion fractionation and reactivity at air/water: methanol interfaces. Implications for the origin of Hofmeister effects. *J. Phys. Chem. B* **2008**, *112*, 7157–7161.

(25) Wilson, M. A.; Pohorille, A.; Pratt, L. R. Molecular dynamics of the water liquid-vapor interface. *J. Phys. Chem.* **1987**, *91*, 4873–4878.

(26) Lee, C.-Y.; McCammon, J. A.; Rossky, P. The structure of liquid water at an extended hydrophobic surface. *J. Chem. Phys.* **1984**, *80*, 4448–4455.

(27) Signorell, R.; Winter, B. Photoionization of the aqueous phase: clusters, droplets and liquid jets. *Phys. Chem. Chem. Phys.* **2022**, *24*, 13438–13460.

(28) Becker, M. R.; Loche, P.; Netz, R. R. Electrokinetic, electrochemical, and electrostatic surface potentials of the pristine water liquid–vapor interface. *J. Chem. Phys.* **2022**, *157*.

(29) Cox, S. J.; Thorpe, D. G.; Shaffer, P. R.; Geissler, P. L. Assessing long-range contributions to the charge asymmetry of ion adsorption at the air–water interface. *Chem. Sci.* **2020**, *11*, 11791–11800.

(30) Enami, S.; Colussi, A. J. Long-range specific ion-ion interactions in hydrogen-bonded liquid films. *J. Chem. Phys.* **2013**, *138*, 184706.

(31) Enami, S.; Colussi, A. J. Ion-Specific Long-Range Correlations on Interfacial Water Driven by Hydrogen Bond Fluctuations. *J. Phys. Chem. B* **2014**, *118*, 1861–1866.

(32) Otten, D. E.; Shaffer, P. R.; Geissler, P. L.; Saykally, R. J. Elucidating the mechanism of selective ion adsorption to the liquid water surface. *Proc. Natl. Acad. Sci. U.S.A.* **2012**, *109*, 701–705.

(33) Onorato, R. M.; Otten, D. E.; Saykally, R. J. Measurement of bromide ion affinities for the air/water and dodecanol/water interfaces at molar concentrations by UV second harmonic generation spectroscopy. *J. Phys. Chem. C* **2010**, *114*, 13746–13751.

(34) Smith, J. W.; Saykally, R. J. Soft x-ray absorption spectroscopy of liquids and solutions. *Chem. Rev.* **2017**, *117*, 13909–13934.

(35) Baer, M. D.; Mundy, C. J. Toward an understanding of the specific ion effect using density functional theory. *J. Phys. Chem. Lett.* **2011**, *2*, 1088–1093.

(36) Adel, T.; Ng, K. C.; Vazquez de Vasquez, M. G.; Velez-Alvarez, J.; Allen, H. C. Insight into the Ionizing Surface Potential Method and Aqueous Sodium Halide Surfaces. *Langmuir* **2021**, *37*, 7863–7874.

(37) Beck, T. L. The influence of water interfacial potentials on ion hydration in bulk water and near interfaces. *Chem. Phys. Lett.* **2013**, *561*, 1–13.

(38) Tobias, D. J.; Hemminger, J. C. Getting specific about specific ion effects. *Science* **2008**, *319*, 1197–1198.

(39) Tielrooij, K.; Garcia-Araez, N.; Bonn, M.; Bakker, H. Cooperativity in ion hydration. *Science* **2010**, *328*, 1006–1009.

(40) Vrbka, L.; Mucha, M.; Minofar, B.; Jungwirth, P.; Brown, E. C.; Tobias, D. J. Propensity of soft ions for the air/water interface. *Current opinion in colloid & interface science* **2004**, *9*, 67–73.

(41) Bastos-González, D.; Pérez-Fuentes, L.; Drummond, C.; Faraudo, J. Ions at interfaces: the central role of hydration and hydrophobicity. *Current opinion in colloid & interface science* **2016**, *23*, 19–28.

(42) Levin, Y. Polarizable ions at interfaces. *Phys. Rev. Lett.* **2009**, *102*, 147803.

(43) Chang, T.-M.; Dang, L. X. Recent advances in molecular simulations of ion solvation at liquid interfaces. *Chem. Rev.* **2006**, *106*, 1305–1322.

(44) Benjamin, I. Theoretical study of ion solvation at the water liquid–vapor interface. *J. Chem. Phys.* **1991**, *95*, 3698–3709.

(45) Markin, V. S.; Volkov, A. G. Quantitative theory of surface tension and surface potential of aqueous solutions of electrolytes. *J. Phys. Chem. B* **2002**, *106*, 11810–11817.

(46) Onuki, A. Ginzburg-Landau theory of solvation in polar fluids: Ion distribution around an interface. *Phys. Rev. E* **2006**, *73*, 021506.

(47) Chakraborty, D.; Patey, G. How crystals nucleate and grow in aqueous NaCl solution. *J. Phys. Chem. Lett.* **2013**, *4*, 573–578.

(48) Ou, S.-C.; Cui, D.; Patel, S. Molecular modeling of ions at interfaces: Exploring similarities to hydrophobic solvation through the lens of induced aqueous interfacial fluctuations. *Phys. Chem. Chem. Phys.* **2016**, *18*, 30357–30365.

(49) Dang, L. X. Computational study of ion binding to the liquid interface of water. *J. Phys. Chem. B* **2002**, *106*, 10388–10394.

(50) Duignan, T. T.; Zhao, X. S. The Born model can accurately describe electrostatic ion solvation. *Physical Chemistry Chemical Physics* **2020**, *22*, 25126–25135.

(51) Noah-Vanhoucke, J.; Geissler, P. L. On the fluctuations that drive small ions toward, and away from, interfaces between polar liquids and their vapors. *Proc. Natl. Acad. Sci. U.S.A.* **2009**, *106*, 15125–15130.

(52) Jubb, A. M.; Hua, W.; Allen, H. C. Environmental chemistry at vapor/water interfaces: insights from vibrational sum frequency generation spectroscopy. *Annu. Rev. Phys. Chem.* **2012**, *63*, 107–130.

(53) Castro, A.; Bhattacharyya, K.; Eisenthal, K. B. Energetics of adsorption of neutral and charged molecules at the air/water interface by second harmonic generation: Hydrophobic and solvation effects. *J. Chem. Phys.* **1991**, *95*, 1310–1315.

(54) Ren, Y.; Soni, A.; Kumar, A.; Bertram, A. K.; Patey, G. Effects of pH on Ice Nucleation by the α-Alumina (0001) Surface. *J. Phys. Chem. C* **2022**, *126*, 19934–19946.

(55) Manciu, M.; Ruckenstein, E. On the interactions of ions with the air/water interface. *Langmuir* **2005**, *21*, 11312–11319.

(56) Hantal, G.; Klíma, M.; McFegan, L.; Kolafa, J.; Jedlovszky, P. Does the Sign of Charge Affect the Surface Affinity of Simple Ions? *J. Phys. Chem. B* **2023**, *127*, 6205–6216.

(57) Briant, C.; Burton, J. Molecular dynamics study of the structure and thermodynamic properties of argon microclusters. *J. Chem. Phys.* **1975**, *63*, 2045–2058.

(58) Wilson, M. A.; Pohorille, A. Interaction of monovalent ions with the water liquid–vapor interface: A molecular dynamics study. *J. Chem. Phys.* **1991**, *95*, 6005–6013.

(59) Markovich, G.; Giniger, R.; Levin, M.; Cheshnovsky, O. Photoelectron spectroscopy of iodine anion solvated in water clusters. *J. Chem. Phys.* **1991**, *95*, 9416–9419.

(60) Markovich, G.; Pollack, S.; Giniger, R.; Cheshnovsky, O. Photoelectron spectroscopy of Cl-, Br-, and I- solvated in water clusters. *J. Chem. Phys.* **1994**, *101*, 9344–9353.

(61) Lu, D.; Singer, S. J. Ion solvation in model polar clusters. *J. Chem. Phys.* **1996**, *105*, 3700–3714.

(62) Perera, L.; Berkowitz, M. L. Many-body effects in molecular dynamics simulations of Na+ (H2O) n and Cl-(H2O) n clusters. *J. Chem. Phys.* **1991**, *95*, 1954–1963.

(63) Perera, L.; Berkowitz, M. L. Erratum: Many-body effects in molecular dynamics simulations of Na+ (H2O) n and Cl-(H2O) n clusters [J. Chem. Phys. 95, 1954 (1991)]. *J. Chem. Phys.* **1993**, *99*, 4236–4237.

(64) Fifen, J. J.; Agmon, N. Structure and spectroscopy of hydrated sodium ions at different temperatures and the cluster stability rules. *J. Chem. Theory Comput.* **2016**, *12*, 1656–1673.

(65) Kelly, C. P.; Cramer, C. J.; Truhlar, D. G. Aqueous solvation free energies of ions and ion- water clusters based on

an accurate value for the absolute aqueous solvation free energy of the proton. *J. Phys. Chem. B* **2006**, *110*, 16066–16081.

(66) Gorlova, O.; DePalma, J. W.; Wolke, C. T.; Brathwaite, A.; Odbadrakh, T. T.; Jordan, K. D.; McCoy, A. B.; Johnson, M. A. Characterization of the primary hydration shell of the hydroxide ion with H2 tagging vibrational spectroscopy of the OH^--(H2O) n= 2, 3 and OD^--(D2O) n= 2, 3 clusters. *J. Chem. Phys.* **2016**, *145*, 134304.

(67) Perera, L.; Berkowitz, M. L. Stabilization energies of Cl-, Br-, and I- ions in water clusters. *J. Chem. Phys.* **1993**, *99*, 4222–4224.

(68) Perera, L.; Berkowitz, M. L. Structure and dynamics of Cl-(H2O) 20 clusters: The effect of the polarizability and the charge of the ion. *J. Chem. Phys.* **1992**, *96*, 8288–8294.

(69) Lynden-Bell, R.; Rasaiah, J.; Noworyta, J. Using simulation to study solvation in water. *Pure Appl. Chem.* **2001**, *73*, 1721–1731.

(70) Bagchi, B.; Jana, B. Solvation dynamics in dipolar liquids. *Chem. Soc. Rev.* **2010**, *39*, 1936–1954.

(71) Miller, D. J.; Lisy, J. M. Hydrated Alkali-Metal Cations: Infrared Spectroscopy and ab Initio Calculations of M+ (H2O) x= 2- 5Ar cluster ions for M= Li, Na, K, and Cs. *J. Am. Chem. Soc.* **2008**, *130*, 15381–15392.

(72) Thaunay, F.; Ohanessian, G.; Clavaguera, C. Dynamics of ions in a water drop using the AMOEBA polarizable force field. *Chem. Phys. Lett.* **2017**, *671*, 131–137.

(73) Burnham, C. J.; Petersen, M. K.; Day, T. J.; Iyengar, S. S.; Voth, G. A. The properties of ion-water clusters. II. Solvation structures of Na+, Cl-, and H+ clusters as a function of temperature. *J. Chem. Phys.* **2006**, *124*, 024327.

(74) Malek, S. M. A.; Kwan, V.; Saika-Voivod, I.; Consta, S. Low Density Interior in Supercooled Aqueous Nanodroplets Expels Ions to the Subsurface. *J. Am. Chem. Soc.* **2021**, *143*, 13113–13123.

(75) Sharma, B.; Chandra, A. Born–Oppenheimer Molecular Dynamics Simulations of a Bromate Ion in Water Reveal Its Dual Kosmotropic and Chaotropic Behavior. *The Journal of Physical Chemistry B* **2018**, *122*, 2090–2101.

(76) Chakrabarty, S.; Williams, E. R. The effect of halide and iodate anions on the hydrogen-bonding network of water in aqueous nanodrops. *Phys. Chem. Chem. Phys.* **2016**, *18*, 25483–25490.

(77) Stachl, C. N.; Williams, E. R. Effects of temperature on Cs+ (H2O) 20 clathrate structure. *J. Phys. Chem. Lett.* **2020**, *11*, 6127–6132.

(78) Muralidharan, A.; Pratt, L.; Chaudhari, M.; Rempe, S. Quasi-chemical theory for anion hydration and specific ion effects: Cl-(aq) vs. F-(aq). *Chem. Phys. Lett.: X* **2019**, *4*, 100037.

(79) Cabarcos, O. M.; Weinheimer, C. J.; Martinez, T. J.; Lisy, J. M. The solvation of chloride by methanol—surface versus interior cluster ion states. *J. Chem. Phys.* **1999**, *110*, 9516–9526.

(80) Laria, D.; Fernández-Prini, R. Molecular dynamics study of water clusters containing ion pairs: From contact to dissociation. *J. Chem. Phys.* **1995**, *102*, 7664–7673.

(81) Corti, H. R.; Appignanesi, G. A.; Barbosa, M. C.; Bordin, J. R.; Calero, C.; Camisasca, G.; Elola, M. D.; Franzese, G.; Gallo, P.; Hassanali, A. et al. Structure and dynamics of

nanoconfined water and aqueous solutions. *Eur. Phys. J. E* **2021**, *44*, 1–50.

(82) Brodskaya, E.; Lyubartsev, A. P.; Laaksonen, A. Molecular dynamics simulations of water clusters with ions at atmospheric conditions. *J. Chem. Phys.* **2002**, *116*, 7879–7892.

(83) Galib, M.; Baer, M.; Skinner, L.; Mundy, C.; Huthwelker, T.; Schenter, G.; Benmore, C.; Govind, N.; Fulton, J. L. Revisiting the hydration structure of aqueous Na+. *J. Chem. Phys.* **2017**, *146*, 084504.

(84) Wang, P.; Shi, R.; Su, Y.; Tang, L.; Huang, X.; Zhao, J. Hydrated sodium ion clusters [Na+ (H2O) n (n= 1–6)]: an ab initio study on structures and noncovalent interaction. *Frontiers in chemistry* **2019**, *7*, 624.

(85) Heindel, J. P.; Xantheas, S. S. The many-body expansion for aqueous systems revisited: II. Alkali metal and halide ion–water interactions. *J. Chem. Theory Comput.* **2021**, *17*, 2200–2216.

(86) Zhao, Y.; Li, H.; Zeng, X. C. First-principles molecular dynamics simulation of atmospherically relevant anion solvation in supercooled water droplet. *J. Am. Chem. Soc.* **2013**, *135*, 15549–15558.

(87) Kolev, S. K.; St. Petkov, P.; Milenov, T. I.; Vayssilov, G. N. Sodium and Magnesium Ion Location at the Backbone and at the Nucleobase of RNA: Ab Initio Molecular Dynamics in Water Solution. *ACS Omega* **2022**, *7*, 23234–23244.

(88) Wise, P. K.; Slipchenko, L. V.; Ben-Amotz, D. Ion-Size Dependent Adsorption Crossover on the Surface of a Water Droplet. *J. Phys. Chem. B* **2023**,

(89) Stuart, S. J.; Berne, B. Effects of polarizability on the hydration of the chloride ion. *J. Phys. Chem.* **1996**, *100*, 11934–11943.

(90) Wick, C. D.; Xantheas, S. S. Computational investigation of the first solvation shell structure of interfacial and bulk aqueous chloride and iodide ions. *J. Phys. Chem. B* **2009**, *113*, 4141–4146.

(91) Herce, D. H.; Perera, L.; Darden, T. A.; Sagui, C. Surface solvation for an ion in a water cluster. *J. Chem. Phys.* **2005**, *122*, 024513.

(92) Caleman, C.; Hub, J. S.; van Maaren, P. J.; van der Spoel, D. Atomistic simulation of ion solvation in water explains surface preference of halides. *Proc. Natl. Acad. Sci. U.S.A.* **2011**, *108*, 6838–6842.

(93) Consta, S.; Kapral, R. Ionization reactions of ion complexes in mesoscopic water clusters. *J. Chem. Phys.* **1999**, *111*, 10183–10191.

(94) Lamoureux, G.; Harder, E.; Vorobyov, I. V.; Roux, B.; MacKerell, A. D. A polarizable model of water for molecular dynamics simulations of biomolecules. *Chem. Phys. Lett.* **2006**, *418*, 245–249.

(95) Oh, M. I.; Malevanets, A.; Paliy, M.; Frenkel, D.; Consta, S. When droplets become stars: charged dielectric droplets beyond the Rayleigh limit. *Soft Matter* **2017**, *13*, 8781–8795.

(96) Rayleigh, L. XX. On the equilibrium of liquid conducting masses charged with electricity. *Philos. Mag.* **1882**, *14*, 184–186.

(97) Hendricks, C.; Schneider, J. Stability of a conducting droplet under the influence of surface tension and electrostatic forces. *Am. J. Phys.* **1963**, *31*, 450–453.

(98) Consta, S.; Malevanets, A. Disintegration mechanisms of charged nanodroplets: novel systems for applying

methods of activated processes. *Mol. Simul.* **2015**, *41*, 73–85.

(99) Onsager, L.; Samaras, N. N. The surface tension of Debye-Hückel electrolytes. *J. Chem. Phys.* **1934**, *2*, 528–536.

(100) Levin, Y. Interfacial tension of electrolyte solutions. *J. Chem. Phys.* **2000**, *113*, 9722–9726.

(101) Wagner, C. The surface tension of dilute solutions of electrolytes. *Phys. Z* **1924**, *25*, 474–477.

(102) Levin, Y.; Dos Santos, A. P.; Diehl, A. Ions at the air-water interface: an end to a hundred-year-old mystery? *Phys. Rev. Lett.* **2009**, *103*, 257802.

(103) Baer, M. D.; Stern, A. C.; Levin, Y.; Tobias, D. J.; Mundy, C. J. Electrochemical surface potential due to classical point charge models drives anion adsorption to the air–water interface. *J. Phys. Chem. Lett.* **2012**, *3*, 1565–1570.

(104) Olivieri, G.; Goel, A.; Kleibert, A.; Cvetko, D.; Brown, M. A. Quantitative ionization energies and work functions of aqueous solutions. *Phys. Chem. Chem. Phys.* **2016**, *18*, 29506–29515.

(105) Kathmann, S. M.; Kuo, I.-F. W.; Mundy, C. J.; Schenter, G. K. Understanding the surface potential of water. *J Phys. Chem. B* **2011**, *115*, 4369–4377.

(106) Kwan, V.; Malevanets, A.; Consta, S. Where do the ions reside in a highly charged droplet? *J. Phys. Chem. A* **2019**, *123*, 9298–9310.

(107) Wagner, W.; Pruß, A. The IAPWS formulation 1995 for the thermodynamic properties of ordinary water substance for general and scientific use. *J. Phys. Chem. Ref. Data* **2002**, *31*, 387–535.

(108) Lemmon, E.; McLinden, M.; Friend, D.; Linstrom, P.; Mallard, W. NIST Standard Reference Database 69: NIST Chemistry WebBook, Thermophysical Properties of Fluid Systems, Isobaric Properties for Water. 2011.

(109) Stukan, M. R.; Asmadi, A.; Abdallah, W. Bulk properties of SWM4-NDP water model at elevated temperature and pressure. *Journal of Molecular Liquids* **2013**, *180*, 65–69.

(110) Jiang, W.; Hardy, D. J.; Phillips, J. C.; MacKerell, A. D.; Schulten, K.; Roux, B. High-Performance Scalable Molecular Dynamics Simulations of a Polarizable Force Field Based on Classical Drude Oscillators in NAMD. *J. Phys. Chem. Lett.* **2011**, *2*, 87–92, PMID: 21572567.

(111) Abascal, J. L. F.; Vega, C. A general purpose model for the condensed phases of water: TIP4P/2005. *J. Phys. Chem* **2005**, *123*, 234505.

(112) Aqvist, J. Ion-water interaction potentials derived from free energy perturbation simulations. *J. Phys. Chem.* **1990**, *94*, 8021–8024.

(113) Jensen, K. P.; Jorgensen, W. L. Halide, ammonium, and alkali metal ion parameters for modeling aqueous solutions. *J. Chem. Theory Comput.* **2006**, *2*, 1499–1509.

(114) Kirby, B. J.; Jungwirth, P. Charge scaling manifesto: A way of reconciling the inherently macroscopic and microscopic natures of molecular simulations. *J. Phys. Chem. Lett.* **2019**, *10*, 7531–7536.

(115) Zeron, I.; Abascal, J.; Vega, C. A force field of Li+, Na+, K+, Mg2+, Ca2+, Cl-, and SO 4 2- in aqueous solution based on the TIP4P/2005 water model and scaled charges for the ions. *J. Chem. Phys.* **2019**, *151*, 134504.

(116) Blazquez, S.; Conde, M.; Abascal, J.; Vega, C. The Madrid-2019 force field for electrolytes in water using TIP4P/2005 and scaled charges: Extension to the ions

F-, Br-, I-, Rb+, and Cs+. *J. Chem. Phys.* **2022**, *156*, 044505.

(117) Phillips, J. C.; Braun, R.; Wang, W.; Gumbart, J.; Tajkhorshid, E.; Villa, E.; Chipot, C.; Skeel, R. D.; Kalé, L.; Schulten, K. Scalable molecular dynamics with NAMD. *J. Comput. Chem.* **2005**, *26*, 1781–1802.

(118) Humphrey, W.; Dalke, A.; Schulten, K. VMD: Visual Molecular Dynamics. *J. Mol. Graphics* **1996**, *14*, 33–38.

(119) Hunjan, J. S.; Eu, B. C. The Voronoi Volume and Molecular Representation of Molar Volume: Equilibrium Simple Fluids. *J. Chem. Phys.* **2010**, *132*.

(120) Willard, A. P.; Chandler, D. Instantaneous liquid interfaces. *J. Phys. Chem. B* **2010**, *114*, 1954–1958.

(121) Sega, M.; Hantal, G.; Fábián, B.; Jedlovszky, P. Pytim: A python package for the interfacial analysis of molecular simulations. 2018.

(122) Sega, M.; Kantorovich, S. S.; Jedlovszky, P.; Jorge, M. The generalized identification of truly interfacial molecules (ITIM) algorithm for nonplanar interfaces. *J. Chem. Phys.* **2013**, *138*.

(123) Hantal, G.; Kolafa, J.; Sega, M.; Jedlovszky, P. Polarization effects at the surface of aqueous alkali halide solutions. *J. Mol. Liq.* **2023**, 122333.

(124) Behroozi, F. A Fresh Look at the Young-Laplace Equation and Its Many Applications in Hydrostatics. *The Physics Teacher* **2022**, *60*, 358–361.

(125) Bett, K.; Cappi, J. Effect of pressure on the viscosity of water. *Nature* **1965**, *207*, 620–621.

(126) Cho, C.-H.; Urquidi, J.; Robinson, G. W. Molecular-level description of temperature and pressure effects on the viscosity of water. *J. Chem. Phys.* **1999**, *111*, 10171–10176.

(127) Malek, S. M. A.; Poole, P. H.; Saika-Voivod, I. Thermodynamic and structural anomalies of water nanodroplets. *Nat. Commun.* **2018**, *9*, 2402.

(128) Lin, F.-Y.; Lopes, P. E.; Harder, E.; Roux, B.; MacKerell Jr, A. D. Polarizable force field for molecular ions based on the classical Drude oscillator. *J. Chem. Inf. Model.* **2018**, *58*, 993–1004.

(129) Yesibolati, M. N.; Laganà, S.; Sun, H.; Beleggia, M.; Kathmann, S. M.; Kasama, T.; Mølhave, K. Mean inner potential of liquid water. *Phys. Rev. Lett.* **2020**, *124*, 065502.

(130) Wilson, M. A.; Pohorille, A.; Pratt, L. R. Comment on "Study on the liquid–vapor interface of water. I. Simulation results of thermodynamic properties and orientational structure". *J. Chem. Phys.* **1989**, *90*, 5211–5213.

(131) Jungwirth, P.; Finlayson-Pitts, B. J.; Tobias, D. J. Introduction: Structure and chemistry at aqueous interfaces. *Chem. Rev.* **2006**, *106*, 1137–1139.

(132) Pearson, R. G. Absolute electronegativity and hardness correlated with molecular orbital theory. *Proc. Natl. Acad. Sci. U.S.A.* **1986**, *83*, 8440–8441.

(133) Pearson, R. G. Absolute electronegativity and hardness: application to inorganic chemistry. *Inorg. Chem.* **1988**, *27*, 734–740.

(134) Fárník, M. Bridging Gaps between Clusters in Molecular-Beam Experiments and Aerosol Nanoclusters. *J. Phys. Chem. Lett.* **2023**, *14*, 287–294.

(135) Pérez, A.; Rubio, A. A molecular dynamics study of water nucleation using the TIP4P/2005 model. *J. Chem. Phys.* **2011**, *135*, 244505.